Osteopontin regulates the functional responses to gas challenge of tumor angiogenesis

Nai-Wei Yao[1,2], Chiao-Chi V. Chen[1], Yi-Hua Hsu[1], Hsiu-Ting Lin[1], Jeou-Yuan Chen[1], and Chen Chang[1]

[1]*Institute of Biomedical Sciences, Academic Sinica, Taipei, Taiwan,* [2]*Department of Zoology, National Taiwan University, Taipei, Taiwan*

Introduction

Angiogenesis, one of the cancer hallmarks, is critical in driving tumor progression and metastasis. Osteopontin (OPN), a member of the small integrin-binding ligand N-linked glycoproteins (SIBLINGs) family, is frequently overexpressed in glioblastoma and its expression is correlated with disease progression[1,2]. To exploit the role of OPN in tumor progression and malignancy, the major goal of the present study is to elucidate the involvement of OPN in tumor angiogenesis, in particular its effect on both the functional and structural characteristics of the tumor vasculature. We studied the role of OPN in tumor angiogenesis in a xenograft glioma model using the rat C6 cells from which OPN expression was knocked down, along with the control knockdown (KD) cells. The functional and structural aspects of the tumor vasculatures were investigated by blood oxygenation level-dependent (BOLD) MRI with gas challenge and steady-state contrast-enhanced (SSCE) MRI, respectively. Our study provides direct *in vivo* evidence supporting a role of OPN in the functionality of tumor vasculature.

Material and Method

The rat C6 cells with OPN-KD or luciferase KD (Luc-KD, serving as control) were established by Lentivirus-based shRNA technology. A volume of 0.6 µL of the cell suspension ($1x10^6$/10 uL in phosphate-beffered saline) was injected into 9-week-old Sprague–Dawley rats on the stereotaxic apparatus using a 30-gauge needle (Hamilton, NV, USA) and a micro-infusion pump (Model 310; KD Scientific, MA, USA). The injection was made at the left striatum [Bregma=0.2mm, lateral=3.0mm, and depth=5.0 mm]. After recovery from surgery, the rats were scanned by a 7-T MRI system. For scanning, rats were anesthetized with isoflurane flowed in air (isoflurane at 5% for induction and 2% for maintenance), fitted in a custom designed head holder, and inserted into the magnet. T2-weighted images (T2WIs) were acquired at 24 days after C6 cells implantation using a fast spin echo sequence with field of view (FOV) =2.56 cm, slice thickness=0.5 mm, 8 slices with no gap to cover the whole tumor, TR=4000 ms, TE=70 ms, echo train length=8, number of excitations (NEX) =12, and matrix size=256×128 (zero filled to 256×256). To determine ΔR2* of gas challenge, T2*-weighted images (T2*WI) were performed while air and carbogen (5% CO_2/95% O_2) inhaling. Acquisition was delayed by 15 minutes after gas transition. T2*WI was acquired using 2D fast low angle shot (FLASH) sequence with a TR=200 ms, a TE=25 ms, flip angle of 25°, FOV=2.56cm*2.56cm, acquisition matrix=256×256 (zero-padded to 512×512). ΔR2* map of gas challenge was calculated pixel-by-pixel by $(1/TE)\ln(S_{carbogen}/S_{Air})$ using commercial available MR Vision (MR Vision Co.). ΔR2, ΔR2*, vascular density, and size were evaluated by SSCE MRI. To determine ΔR2 and ΔR2* maps, T2-weighted spin-echo and T2*-weighted gradient echo pulse sequences, respectively, were performed before and after an injection of monocrystalline iron oxide nanocolloid (MION) at a dose of 15 mg Fe/kg via the tail vein. ΔR2 and ΔR2* maps were calculated pixel-by-pixel by $(1/TE)\ln(S_{pre}/S_{post})$ using MR Vision. These two parameters can be further derived to provide information on vessel size (ΔR2*/ΔR2) and density (ΔR2 /(ΔR2*) $^{2/3}$). T2- and T2*WIs were obtained with the same geometry with an FOV=2.56 cm×2.56 cm, matrix size=256×128 (zero filled to 256×256), and 1-mm-thick slice. For the T2WI in SSCE MRI, the same protocol described above was used. T2*WI used a FLASH sequence with TR=300 ms, TE=13 ms, flip angle=15°, and NEX = 16. Student t-test was used to identify group differences using STATVIEW.

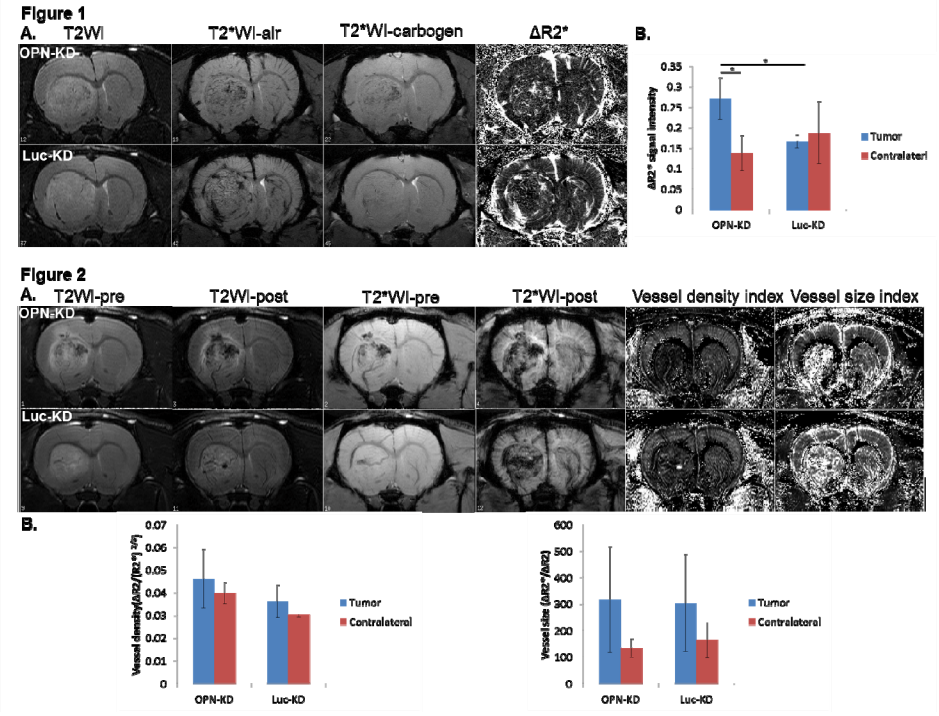

Results and Discussion

Fig. 1A shows the T2WI, T2*WI with air, T2*WI with carbogen, and the ΔR2* maps. T2WI showed that the tumor sizes were invariable, but the T2*WI and ΔR2* maps demonstrate that the OPN-KD tumor showed higher reactivity to the gas challenge. The ΔR2* quantification was summarized in Fig. 1B. The ΔR2* signals of OPN-KD tumors were significantly higher than those in Luc-KD tumors ($p<0.05$). The hyperintensities on the ΔR2* maps may indicate the locations of functional vessels with oxygenation ability. According to the results, OPN-KD tumor exhibited significantly more functional intratumor vessels than the control tumor. In contrast, no unequivocal difference was identified in the structural features between OPN-KD and Luc-KD tumor vasculature such as vessel size and density (Images shown as Fig. 2A; Quantification summarized in Fig. 2B). In conclusion, the knockdown of OPN affects the functionality of tumor angiogenesis but preserves the structural features of tumor vasculature. The particular involvement of OPN in tumor angiogenesis provides an insight to the development of anti-tumor treatment

Reference: ***1.*** **Matusan-Ilijas K et al., 2008.** ***2.*** **Saitoh Y et al., 1995.**